Cell Reports, Volume *41*

Supplemental information

Sex differences in resilience to ferroptosis underlie sexual dimorphism in kidney injury and repair

Shintaro Ide, Kana Ide, Koki Abe, Yoshihiko Kobayashi, Hiroki Kitai, Jennifer McKey, Sarah A. Strausser, Lori L. O'Brien, Aleksandra Tata, Purushothama Rao Tata, and Tomokazu Souma

SUPPLEMENTARY FIGURES:

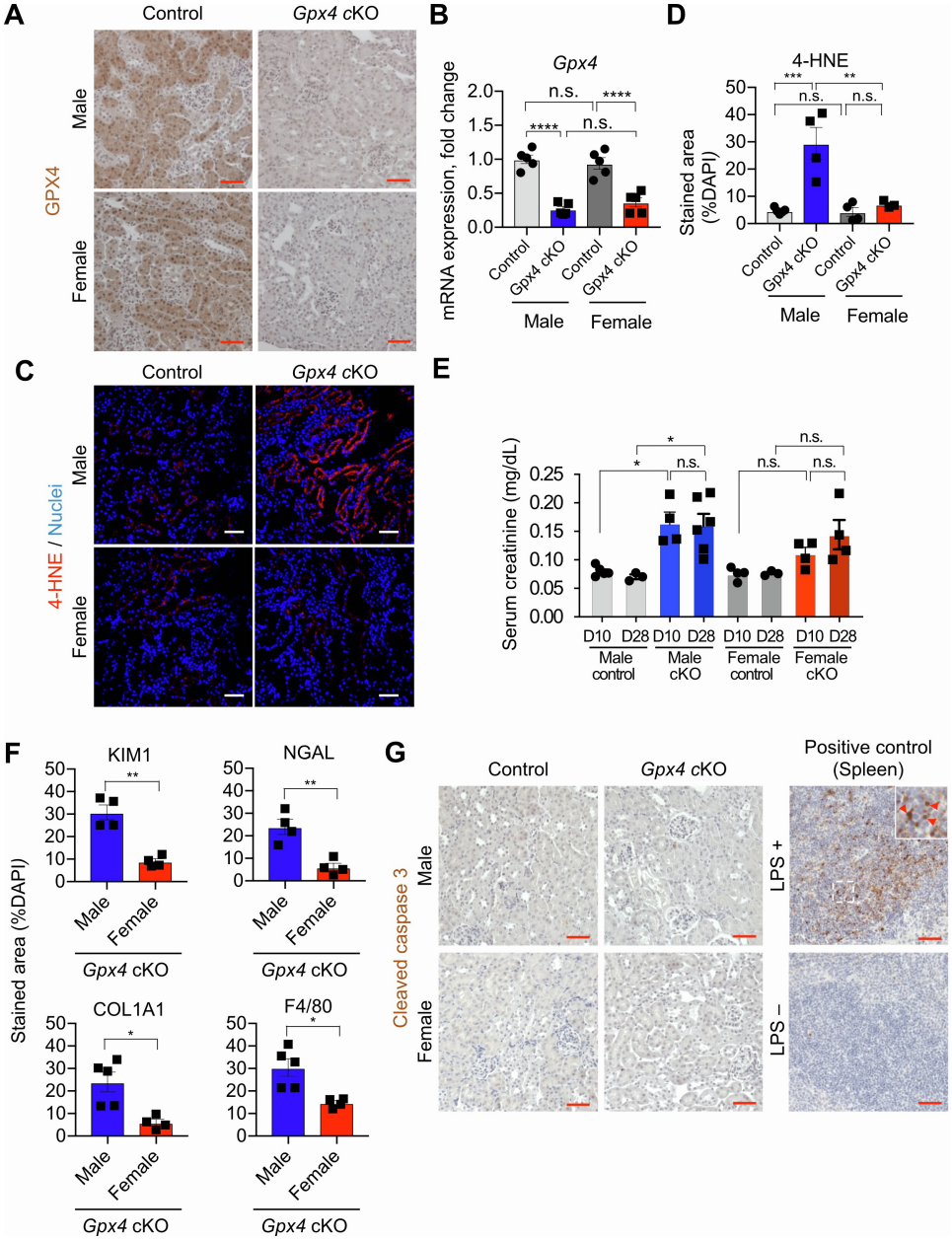

Fig. S1. Female kidneys are protected from ferroptosis and ferroptotic stress. Related to Figure 1. (**A** and **B**) Immunohistochemistry and qPCR analyses for GPX4 expression. N=5. Note that GPX4 is deleted at a comparable level between sexes. N=5. (**C** and **D**) Immunofluorescence for 4-HNE and its quantification. N=3-5. (**E**) Serum creatinine levels for days 10 (D10) and 28 (D28) after initiating doxycycline feeding. (**F**) Quantification of indicated protein expression. See images in Fig. 1D. N=4-5. (**G**) Cleaved caspase 3 staining for evaluating apoptosis. LPS-induced apoptosis of splenocytes was used as a positive control. N=3-4. One-way ANOVA with post hoc multiple comparison test for (B), (D), and (E). Student's t-test for (F). n.s., not significant. *$p < 0.05$; **$p < 0.01$; ***$p < 0.001$; ****$p < 0.0001$. Scale bars: 50 μm in (A), (C), and (G).

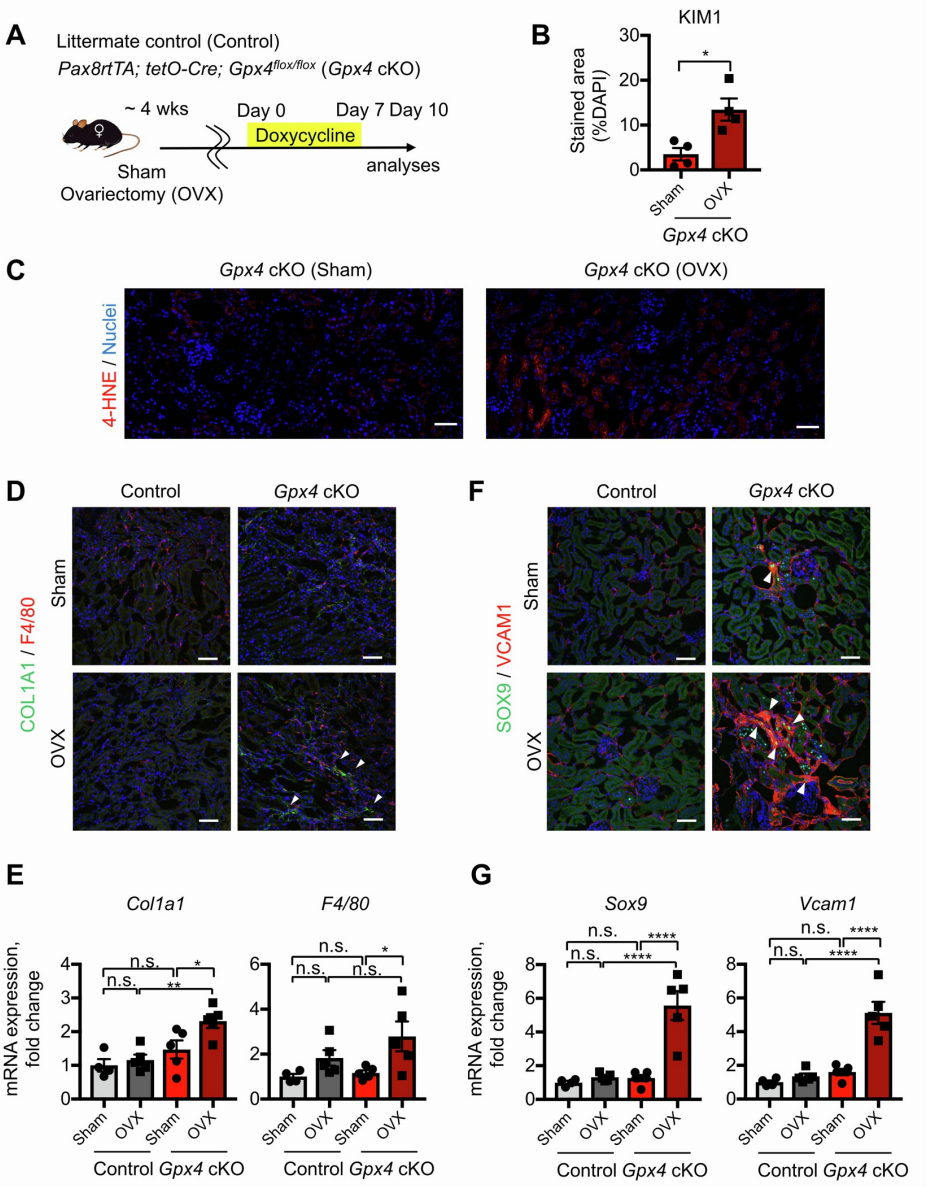

Fig. S2. Intact ovarian function underlies female ferroptosis resilience. Related to Figure 2. (**A**) Experimental workflow for testing ovarian function in female ferroptosis resistance by ovariectomy (OVX). Animals were allowed to recover for 4 weeks after OVX and then treated with doxycycline for 7 days to delete *Gpx4*. Kidneys were harvested on day 10. Control, *Gpx4*-intact control genotype. Sham, sham-operated mice. (**B**) Quantification of KIM1 immunofluorescence in Fig. 2C. N=4. (**C**) Immunofluorescence for 4-HNE. (**D**) Immunofluorescence for COL1A1 and F4/80. Arrowheads, collagen 1A1 deposits. N=4-5. (**E**) Real-time PCR analyses of indicated gene expression. N=4-5. (**F**) Immunofluorescence for SOX9 and VCAM1. Arrowheads, double-positive cells. N=3-4. (**G**) Real-time PCR analyses of indicated gene expression. N=4-5. Student's t-test for (B) and one-way ANOVA with post hoc multiple comparison test for (E) and (G). n.s., not significant. *p < 0.05; **p < 0.01; ***p < 0.001; ****p < 0.0001. Scale bars: 50 μm.

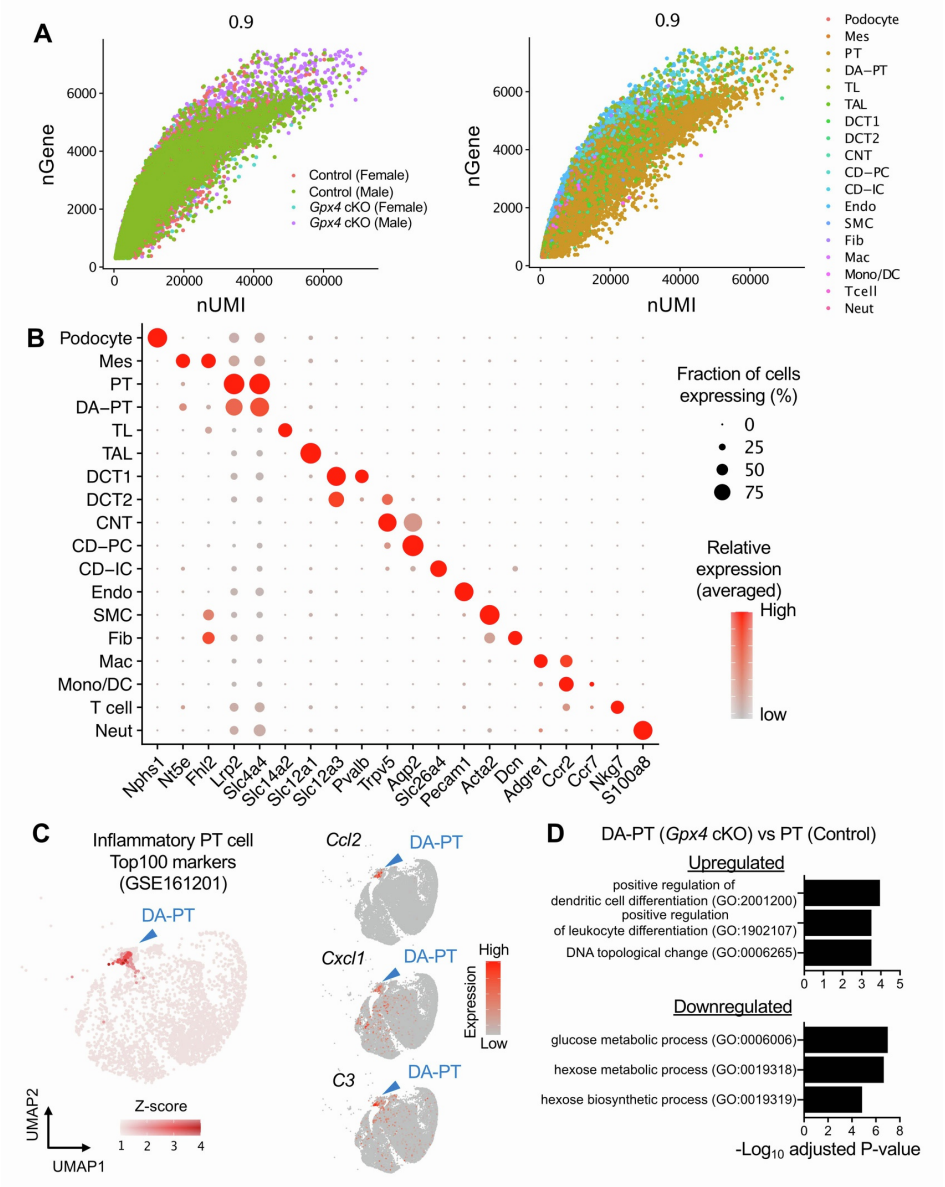

Fig. S3. scRNA sequencing recovers all major cell types in the kidneys. Related to Figure 3. (A) Pearson correlation plots showing the linear relationship between the number of genes (nGene) and unique molecular identifiers (nUMI). Sample conditions and cell types are color-coded. (**B**) Dot plot diagram shows gene expression patterns of cluster-enriched canonical markers. Abbrev. PT, proximal tubule; DA-PT, damage-associated PT; TL, thin limb; TAL, thick ascending limb; DCT, distal convoluted tubule; CNT, connecting tubule; CD, collecting duct (PC, principal cells, IC, intercalated cells); Mes, mesangial cells; Endo, endothelial cells; SMC, smooth muscle cells; Fib, fibroblasts; Mac, macrophages; Mono/DC, monocytes and dendritic cells, Neut, neutrophils. (**C**) UMAP rendering of genes that characterizes inflammatory PT cells after IRI. We obtained Top 100 genes representing inflammatory PT cells from our previous publication (Ide et al., 2021). Right panels: UMAP plots showing proinflammatory genes highly expressed in inflammatory PT cells after IRI (Gerhardt et al., 2021; Ide *et al.*, 2021; Kirita et al., 2020). (**D**) Gene ontology (GO) enrichment analyses. DA-PT cells from *Gpx4* cKO male mice are enriched for proinflammatory signaling compared to normal male PT cells.

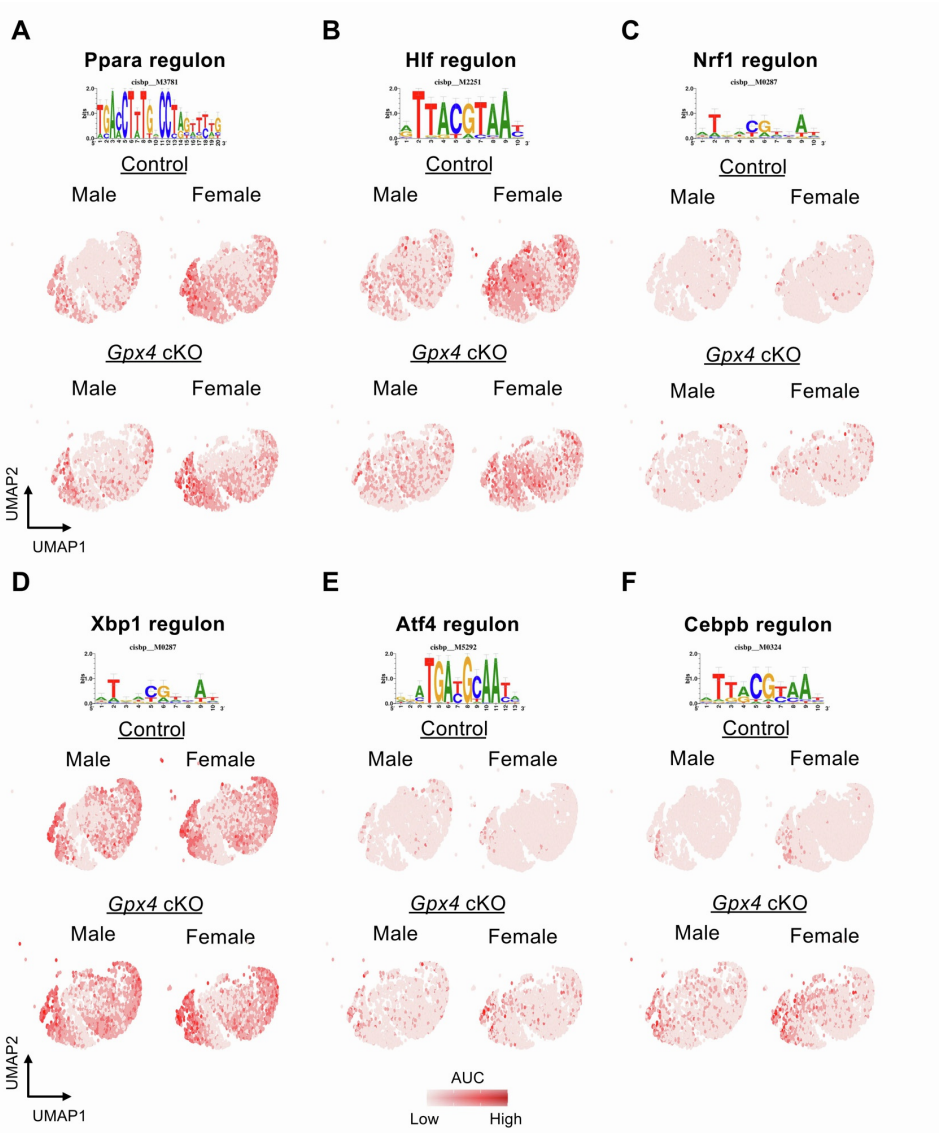

Fig. S4. SCENIC analyses identify potential regulatory nodes that underpin PT cell states in the ferroptotic process. Related to Figure 4. Regulon activities for indicated transcription factors are shown on UMAP of PT cells (red dots represent cells with high regulon activities). AUC; enrichment score for each regulon's activity. Peroxisome proliferator activated receptor alpha (PPARα) is a critical regulator of fatty acid oxidation, lipid remodeling, and mitochondrial function (Clark and Parikh, 2021; Stadler et al., 2015). Hlf regulates antioxidative cellular response in leukemic cells (Roychoudhury et al., 2015). Nrf1 (NFE2L1) regulates lipid metabolism, antioxidative stress responses, and proteostasis (Pakos-Zebrucka et al., 2016), and it protects cardiomyocytes, cancer cells, and adipocytes from ferroptosis (Baird et al., 2017; Cui et al., 2021; Forcina et al., 2022; Hirotsu et al., 2012; Kotschi et al., 2022). Xbp1, Atf4, and Cebpb regulate integrated stress responses and unfolded protein responses to counteract cellular stressors (Kaspar et al., 2021; Pakos-Zebrucka *et al.*, 2016). They are implicated in ferroptosis in cancer cell lines (Dixon et al., 2014; Lin et al., 2021).

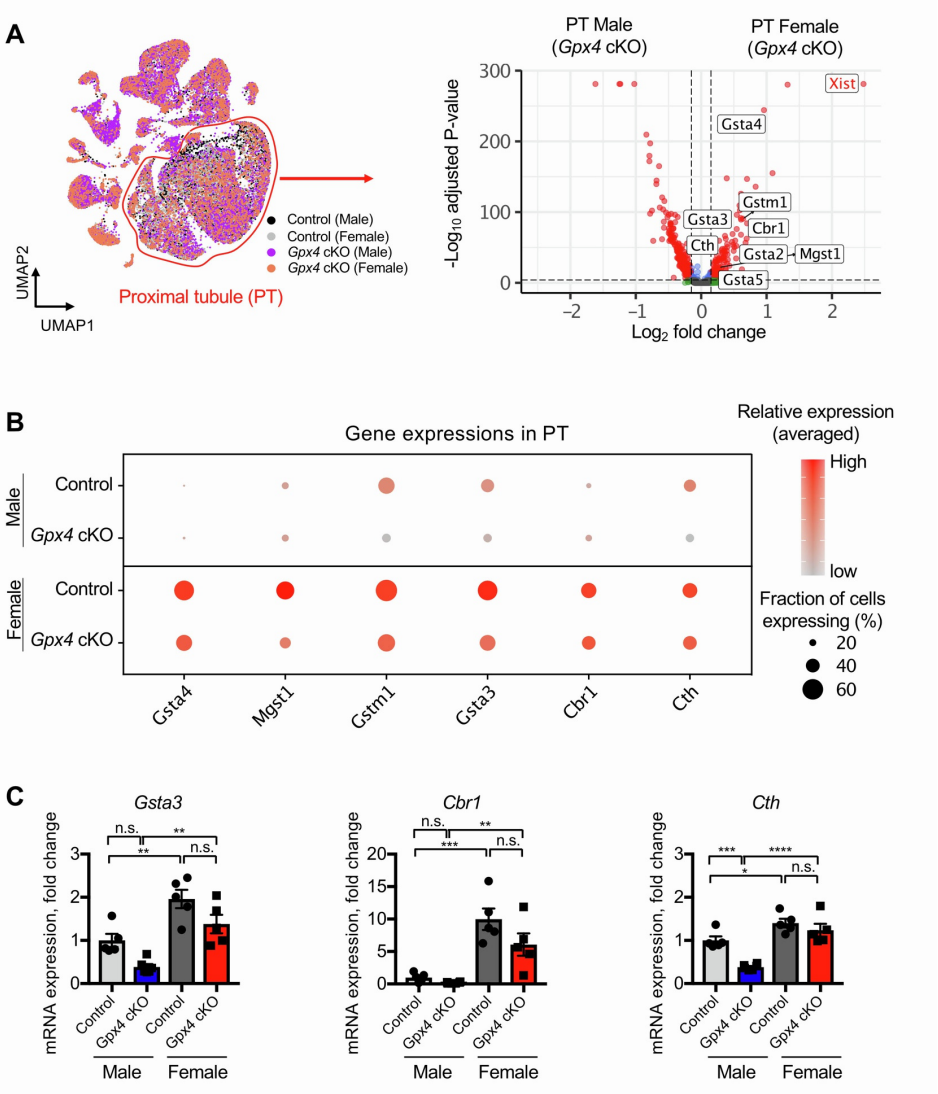

Fig. S5. Differential gene expression analyses identify potential female resilience genes. Related to Figure 4. (A) Volcano plot showing a differentially regulated genes in male and female PT cells of *Gpx4* cKO mice. *Xist* (X-inactive specific transcript) is a long non-coding RNA and expressed in female cells to achieve X-chromosome inactivation. (**B**) Dot plots showing the indicated genes. These genes are highly expressed in female PT cells. Expression patterns of indicated sexually dimorphic genes in normal kidneys (control) were confirmed by Kidney Cell Explorer (Ransick et al., 2019). (**C**) Real-time PCR analyses of indicated gene expression. N=5-6. One-way ANOVA with post hoc multiple comparison test for (C). n.s., not significant. *$p < 0.05$; **$p < 0.01$; ***$p < 0.001$; ****$p < 0.0001$.

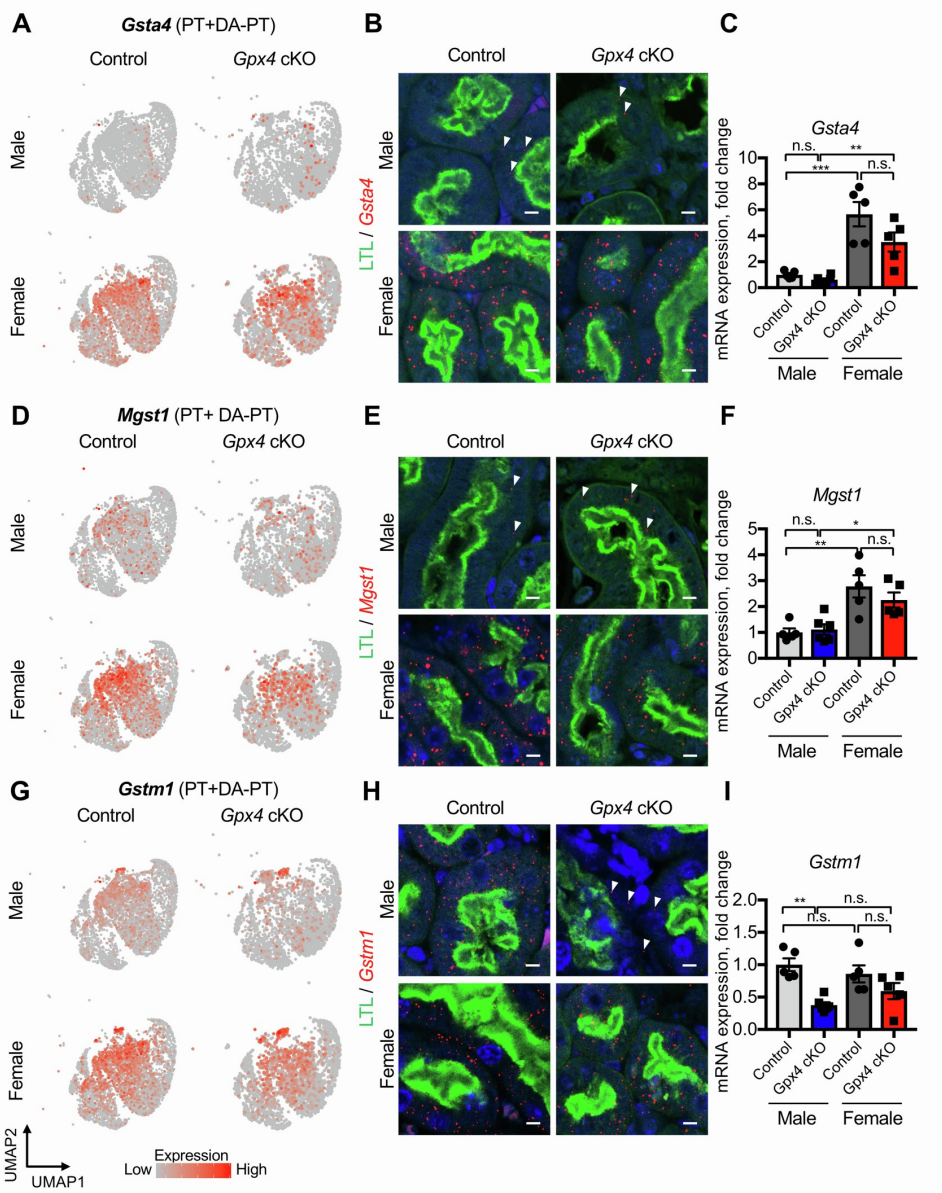

Figure S6. NRF2-target genes are differentially regulated in PT cells between sexes. Related to Figure 4. (**A-C**) Expression of *Gsta4* is shown in UMAP plot (A), by *in situ* hybridization (RNAScope, red dots, B), and quantified by real-time PCR (C). LTL (lotus tetragonolobus lectin) binds the brush border of proximal tubular cells. (**D-F**) Expression of *Mgst1* is shown in UMAP plot (D), by *in situ* hybridization (RNAScope, red dots, E), and quantified by real-time PCR (F). (**G-I**) Expression pattern of *Gstm1* is shown in UMAP plot (G), by *in situ* hybridization (RNAScope, red dots, H), and quantified by real-time PCR (I). Abbrev. PT, proximal tubule, DA-PT, damage-associated proximal tubule. For RNAScope analyses, representative images are shown (N=3). Arrowheads, a few transcripts were detected in male PT cells. Note much higher expressions of indicated transcripts in female PT cells (red dots). N=5-6 for real-time PCR. Scale bars, 5 μm in (B, E, H). One-way ANOVA with post hoc multiple comparison test. n.s., not significant. *$p < 0.05$; **$p < 0.01$; and ***$p < 0.001$.

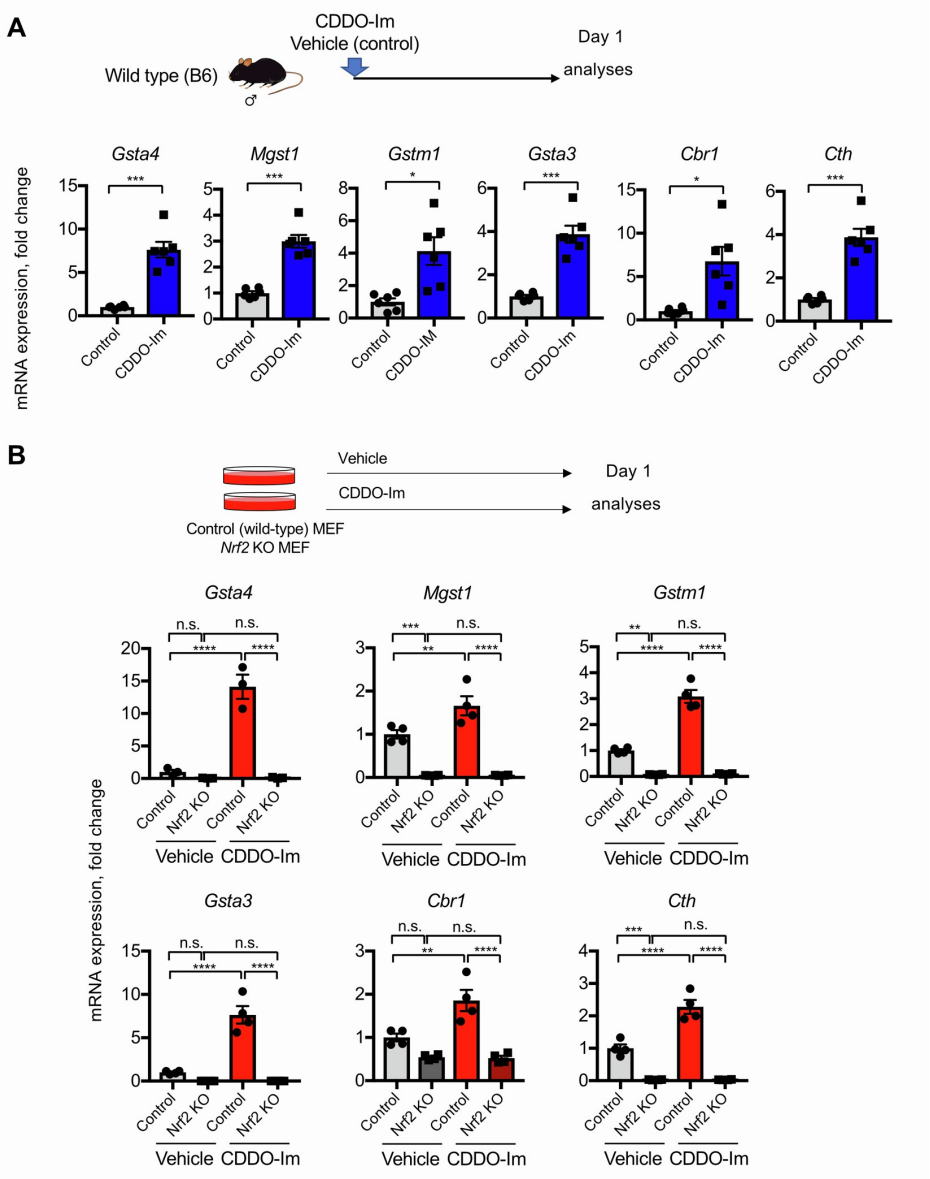

Fig. S7. CDDO-Im, a potent NRF2 inducer, effectively induce potential female resilience genes in male kidneys. Related to Figure 4. (A) Real-time PCR analyses of indicated gene expression in mouse kidneys. N=6. Kidneys were harvested 24 hours after mice were treated with CDDO-Im or vehicle by oral gavage. (**B**) Real-time PCR analyses of indicated gene expression in mouse embryonic fibroblasts (MEFs). Wild-type (control) and *Nrf2* knockout MEFs were treated with either vehicle or CDDO-Im. N=3-4. Note that CDDO-Im effectively induce mRNA expression of these genes in WT but not in *Nrf2* knockout MEFs. Student's t-test for (A) and one-way ANOVA with post hoc multiple comparison test for (B). n.s., not significant. *p < 0.05; **p < 0.01; ***p < 0.001; ****p < 0.0001.

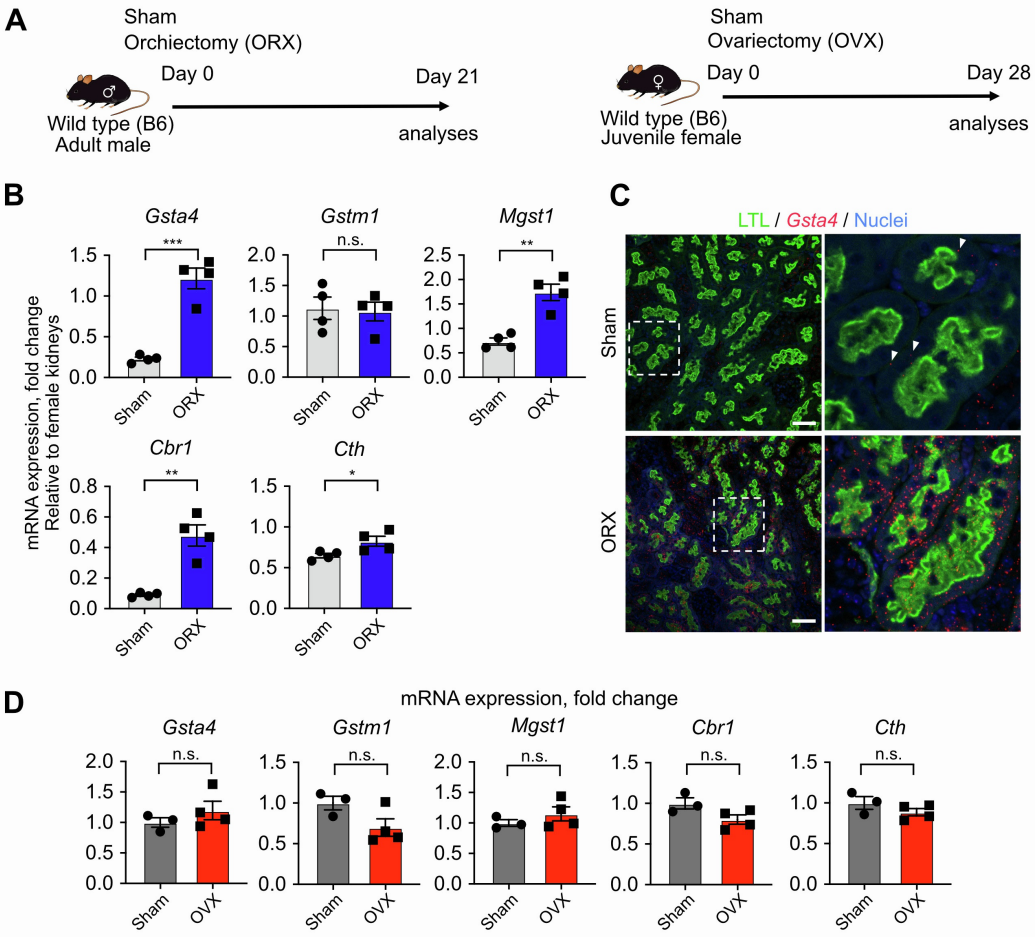

Fig. S8. Gonadectomy identifies the effects of sex hormones on glutathione metabolic gene expressions. Related to Figure 4. (A) Experimental workflow. Wild type C57BL/6J mice were subjected to gonadectomy. Androgens are known to affect renal development; thus, we performed orchiectomy on adult male mice (ages 7-9 weeks old). (**B**) Real-time PCR analyses of indicated gene expression. Note that orchiectomy (ORX) induced robust upregulation glutathione metabolic gene expressions. N=4. (**C**) *In situ* hybridization (RNAScope, red dots) for *Gsta4* expression. Lotus tetragonolobus lectin (LTL), a proximal tubular cell marker. Representative images are shown (N=3). Scale bars: 50 μm. (**D**) Real-time PCR analyses of indicated gene expression. Note that there were no significant effects on these gene expressions by ovariectomy (OVX). N=3-4. Student's t-test for (B) and (D). n.s., not significant. *$p < 0.05$; **$p < 0.01$; ***$p < 0.001$.

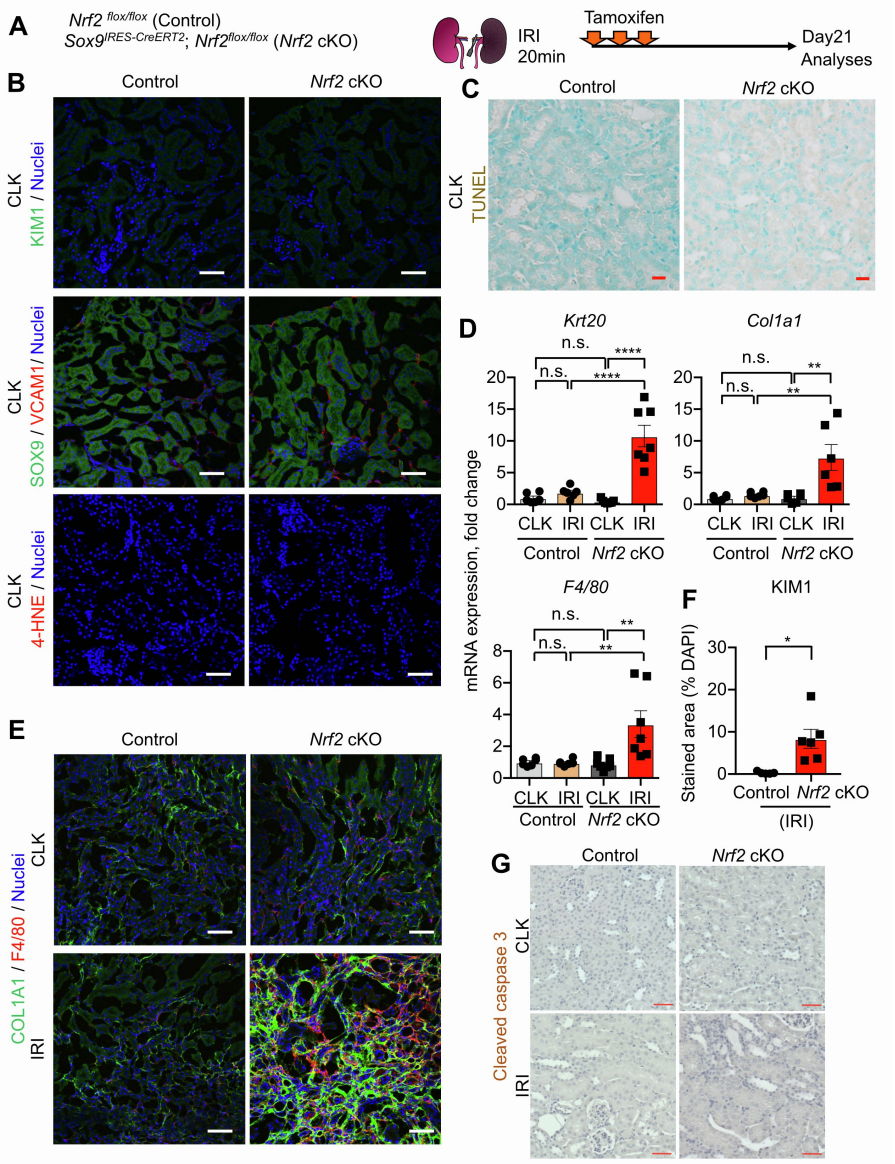

Fig. S9. *Nrf2* deletion prevents successful renal repair after IRI. Related to Figure 5 and 6. (A) Experimental workflow for testing Nrf2 function in regulating PT cell fate after IRI. *Nrf2* cKO mice and their littermate controls (control) were subjected to the same ischemic stress (20 min) and tamoxifen treatment. (**B**) Immunofluorescence for indicated proteins. Contralateral uninjured kidneys (CLK) data are shown. See images for ischemia-reperfusion-injured (IRI) kidneys in Fig. 5, B, C, and F (all are imaged under the same microscopic settings). Note that there were no expression changes in CLK by genetic deletion of *Nrf2*. (**C**) TUNEL staining of kidneys. CLK data are shown. See images for IRI kidneys in Fig. 5H. Note that there were no TUNEL^{+} cells in CLK. (**D**) Real-time PCR analyses of indicated gene expression. N=6-7. (**E**) Immunofluorescence for collagen 1A1 and F4/80. F4/80 is a macrophage marker in mouse kidneys and encoded by *Adgre1* gene. N=4-5. (**F**) Quantification of KIM1 immunofluorescence in Figure 5B. N=5-6. (**G**) Immunostaining for cleaved caspase 3 for evaluating apoptosis (N=2). Student's t-test for (F) and one-way ANOVA with post hoc multiple comparison test for (D). n.s., not significant. *p < 0.05; **p < 0.01; ***p < 0.001; ****p < 0.0001. Scale bars: 50 μm in (B, E and G); 20 μm in (C).

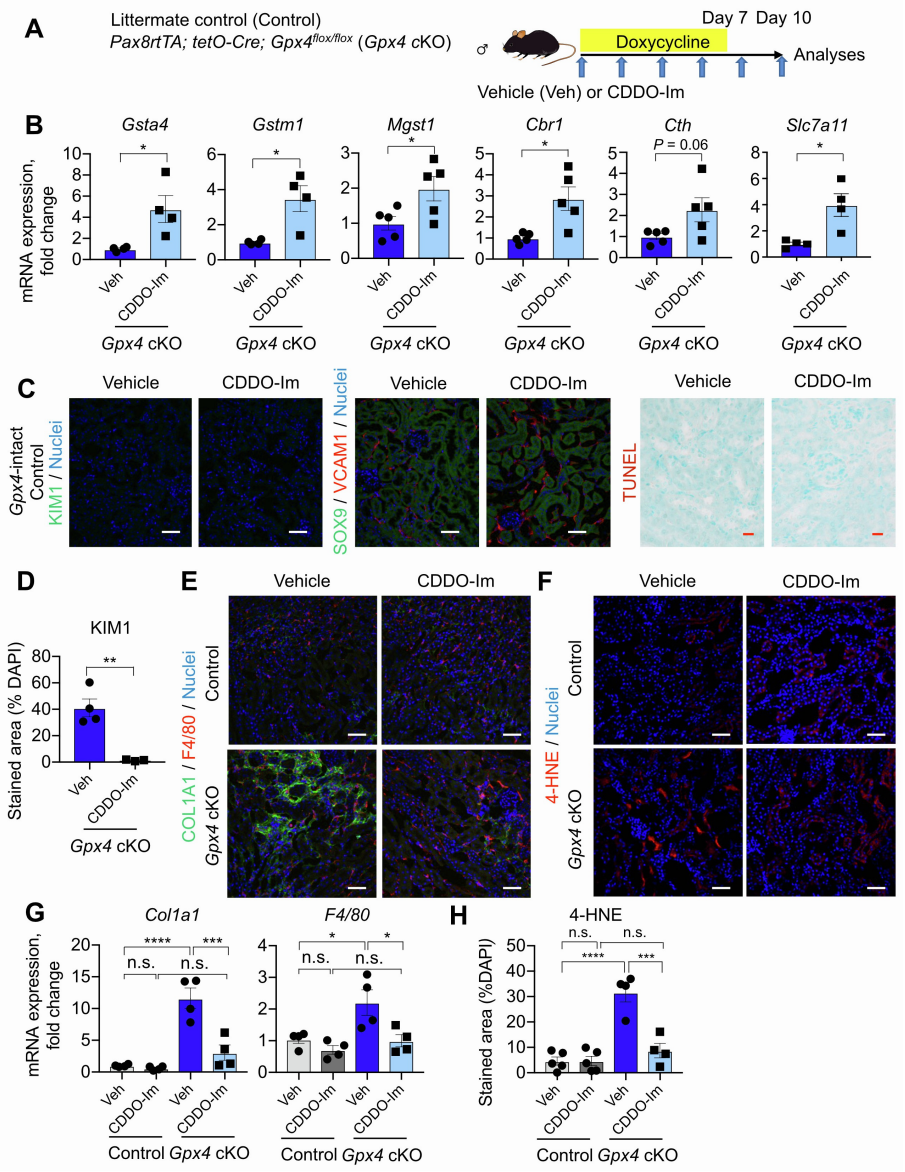

Fig. S10. Pharmacological NRF2 activation prevents ferroptosis in *Gpx4*-deficient male kidneys. Related to Figure 7. (A) Experimental workflow for testing NRF2 function in regulating ferroptotic stress and ferroptosis using *Gpx4* cKO mice. *Gpx4* cKO mice were administered either vehicle (Veh) or CDDO-Im (NRF2 inducer) on alternate days. Doxycycline was given for 7 days, and mice were harvested on day 10. **(B)** Real-time PCR analyses of indicated gene expression. N=4-5. **(C)** Immunofluorescence for indicated proteins and TUNEL staining. *Gpx4*-intect control littermate data are shown. See Fig. 7 for *Gpx4* cKO mice. Note that CDDO-Im did not change expression patterns in *Gpx4*-intact control kidneys. **(D)** Quantification of KIM1 immunofluorescence in Figure 7C. N=3-4. € Immunofluorescence for COL1A1 and F4/80. N=3-4. **(F)** Immunofluorescence for 4-HNE. **(G)** Real-time PCR analyses of indicated gene expression. N=4. **(H)** Quantification for the 4-HNE stained area in (F). N=4-5. Student's t-test for (B) and (D), and one-way ANOVA with post hoc multiple comparison test for (G) and (H). n.s., not significant. *p < 0.05; **p < 0.01; ***p < 0.001; ****p < 0.0001. Scale bars: 50 μm in (C, E, and F); 20 μm in (C, TUNEL).

SUPPLEMENTARY TABLE 1: Genotyping Primers, Related to STAR methods.

Pax8rtTA, Fw: CTCCAGGCCACATATGATTAG

Pax8rtTA, Rv: CCATGTCTAGACTGGACAAGA

Cre, Fw: GTGCAAGTTGAATAACCGGAAATGG,

Cre, Rv: AGAGTCATCCTTAGCGCCGTAAATCAAT

Gpx4 ^{flox}, wt: CTGCAACAGCTCCGAGTTC

Gpx4 ^{flox}, common: CGGTGCCAAAGAAAGAAAGT

Gpx4 ^{flox}, mut: CCAGTAAGCAGTGGGTTCTC

Nrf2 ^{flox}, Fw: TCATGAGAGCTTCCCAGACTC

Nrf2 ^{flox}, Rv: CAGCCAGCTGCTTGTTTTC

Rosa26^{tdTomato}, Fw: CTGTTCCTGTACGGCATGG

Rosa26^{tdTomato}, Rv-GGCATTAAAGCAGCGTATCC

Rosa26^{wt}, Fw: AAGGGAGCTGCAGTGGAGTA

Rosa26^{wt}, Rv: CCGAAAATCTGTGGGAAGTC.

SUPPLEMENTARY TABLE 2: Primers for Quantitative PCR, Related to STAR methods.

Gpx4:	Fw- CCATGCACGAATTCTCAGCC, Rv- GGTGACGATGCACACGAAAC
Sox9:	Fw-GAGCCGGATCTGAAGAGGGA, Rv-GCTTGACGTGTGGCTTGTTC
Vcam1:	Fw-TCTTACCTGTGCGCTGTGAC, Rv-ACTGGATCTTCAGGGAATGAGT
Kim1 (Havcr1):	Fw-AAACCAGAGATTCCCACACG, Rv-GTCGTGGGTCTTCCTGTAGC
Ngal (Lcn2):	Fw-CAAGCAATACTTCAAAATTACCCTGTA, Rv-GCAAAGCGGGTGAAACGTT
Krt20:	Fw-AGCTGAGACGCACCTACCAG, Rv-TGCGCTCCAGAGACTCTTTC
Col1a1:	Fw-AGACATGTTCAGCTTTGTGGAC, Rv-GCAGCTGACTTCAGGGATG
F4/80 (*Adgre1*):	Fw-CCTGGACGAATCCTGTGAAG, Rv-GGTGGGACCACAGAGAGTTG
Gsta4:	Fw-CCCCTGTACTGTCCGACTTC, Rv-AGGAATGTTGCTGATTCTTGTCT
Mgst1:	Fw- GCACTGACGAGAAGGTGGAA, Rv- GATGCCGAGAAAGGGAACGA
Gstm1:	Fw-CCTATGATACTGGGATACTGGAACG, Rv-GGAGCGTCACCCATGGTG
Gsta3:	Fw-TGACCTGGCAAGGTTACGAA, Rv-CGTCGATCTCTACCATGGGC
Cbr1:	Fw-CCTTCCACATTCAAGCAGAGG, Rv-CTCACCATGCTGGACACATTC
Cth:	Fw-CTTTGCATCGGGTCTTGCTG, Rv-CAGATGCCACCCTCCTGAAG
Slc7a11:	Fw-CCCAGATATGCATCGTCCTT, Rv-CGAGTAAAGAGAGAGGACAACCA
18S rRNA:	Fw-CGGCTACCACATCCAAGGAA, Rv-GCTGGAATTACCGCGGCT

SUPPLEMENTARY REFERENCES

Baird, L., Tsujita, T., Kobayashi, E.H., Funayama, R., Nagashima, T., Nakayama, K., and Yamamoto, M. (2017). A Homeostatic Shift Facilitates Endoplasmic Reticulum Proteostasis through Transcriptional Integration of Proteostatic Stress Response Pathways. Mol Cell Biol *37*. 10.1128/MCB.00439-16.

Clark, A.J., and Parikh, S.M. (2021). Targeting energy pathways in kidney disease: the roles of sirtuins, AMPK, and PGC1alpha. Kidney Int *99*, 828-840. 10.1016/j.kint.2020.09.037.

Cui, M., Atmanli, A., Morales, M.G., Tan, W., Chen, K., Xiao, X., Xu, L., Liu, N., Bassel-Duby, R., and Olson, E.N. (2021). Nrf1 promotes heart regeneration and repair by regulating proteostasis and redox balance. Nat Commun *12*, 5270. 10.1038/s41467-021-25653-w.

Dixon, S.J., Patel, D.N., Welsch, M., Skouta, R., Lee, E.D., Hayano, M., Thomas, A.G., Gleason, C.E., Tatonetti, N.P., Slusher, B.S., and Stockwell, B.R. (2014). Pharmacological inhibition of cystine-glutamate exchange induces endoplasmic reticulum stress and ferroptosis. Elife *3*, e02523. 10.7554/eLife.02523.

Forcina, G.C., Pope, L., Murray, M., Dong, W., Abu-Remaileh, M., Bertozzi, C.R., and Dixon, S.J. (2022). Ferroptosis regulation by the NGLY1/NFE2L1 pathway. Proc Natl Acad Sci U S A *119*, e2118646119. 10.1073/pnas.2118646119.

Gerhardt, L.M.S., Liu, J., Koppitch, K., Cippa, P.E., and McMahon, A.P. (2021). Single-nuclear transcriptomics reveals diversity of proximal tubule cell states in a dynamic response to acute kidney injury. Proc Natl Acad Sci U S A *118*. 10.1073/pnas.2026684118.

Hirotsu, Y., Hataya, N., Katsuoka, F., and Yamamoto, M. (2012). NF-E2-related factor 1 (Nrf1) serves as a novel regulator of hepatic lipid metabolism through regulation of the Lipin1 and PGC-1beta genes. Mol Cell Biol *32*, 2760-2770. 10.1128/MCB.06706-11.

Ide, S., Kobayashi, Y., Ide, K., Strausser, S.A., Abe, K., Herbek, S., O'Brien, L.L., Crowley, S.D., Barisoni, L., Tata, A., et al. (2021). Ferroptotic stress promotes the accumulation of pro-inflammatory proximal tubular cells in maladaptive renal repair. Elife *10*, e68603. 10.7554/eLife.68603.

Kaspar, S., Oertlin, C., Szczepanowska, K., Kukat, A., Senft, K., Lucas, C., Brodesser, S., Hatzoglou, M., Larsson, O., Topisirovic, I., and Trifunovic, A. (2021). Adaptation to mitochondrial stress requires CHOP-directed tuning of ISR. Sci Adv *7*. 10.1126/sciadv.abf0971.

Kirita, Y., Wu, H., Uchimura, K., Wilson, P.C., and Humphreys, B.D. (2020). Cell profiling of mouse acute kidney injury reveals conserved cellular responses to injury. Proc Natl Acad Sci U S A *117*, 15874-15883. 10.1073/pnas.2005477117.

Kotschi, S., Jung, A., Willemsen, N., Ofoghi, A., Proneth, B., Conrad, M., and Bartelt, A. (2022). NFE2L1-mediated proteasome function protects from ferroptosis. Mol Metab *57*, 101436. 10.1016/j.molmet.2022.101436.

Lin, C.C., Ding, C.C., Sun, T., Wu, J., Chen, K.Y., Zhou, P., and Chi, J.T. (2021). The regulation of ferroptosis by MESH1 through the activation of the integrative stress response. Cell Death Dis *12*, 727. 10.1038/s41419-021-04018-7.

Pakos-Zebrucka, K., Koryga, I., Mnich, K., Ljujic, M., Samali, A., and Gorman, A.M. (2016). The integrated stress response. EMBO Rep *17*, 1374-1395. 10.15252/embr.201642195.

Ransick, A., Lindstrom, N.O., Liu, J., Zhu, Q., Guo, J.J., Alvarado, G.F., Kim, A.D., Black, H.G., Kim, J., and McMahon, A.P. (2019). Single-Cell Profiling Reveals Sex, Lineage, and Regional Diversity in the Mouse Kidney. Dev Cell *51*, 399-413 e397. 10.1016/j.devcel.2019.10.005.

Roychoudhury, J., Clark, J.P., Gracia-Maldonado, G., Unnisa, Z., Wunderlich, M., Link, K.A., Dasgupta, N., Aronow, B., Huang, G., Mulloy, J.C., and Kumar, A.R. (2015). MEIS1 regulates an HLF-oxidative stress axis in MLL-fusion gene leukemia. Blood *125*, 2544-2552. 10.1182/blood-2014-09-599258.

Stadler, K., Goldberg, I.J., and Susztak, K. (2015). The evolving understanding of the contribution of lipid metabolism to diabetic kidney disease. Curr Diab Rep *15*, 40. 10.1007/s11892-015-0611-8.